Materials Letters 383 (2025) 138013

Contents lists available at ScienceDirect

Materials Letters

journal homepage: www.elsevier.com/locate/matlet

Synergistic functionalization and Cu substitution in Mn-based Prussian blue analogues for high-voltage and high-capacity aqueous zinc-ion battery cathodes

Ruda Jian, Zhuoxun Zhang, Amirarsalan Mashhadian, Roma Avhad, Yun Hao, Shuang Cui, Guoping Xiong *

Department of Mechanical Engineering, The University of Texas at Dallas, 800 W Campbell Rd, Richardson, TX 75080, United States

ARTICLE INFO

Keywords:
Zn-ion batteries
Prussian blue analogue
Cathode materials
High discharge plateau
High capacity

ABSTRACT

Aqueous zinc-ion batteries (AZIBs) are gaining attention for electrochemical energy storage due to their low cost, safety, and environmental compatibility. However, developing cathode materials with simultaneously high capacity and operating voltage to improve energy densities of AZIBs remains a daunting challenge. In this work, new manganese-based Prussian blue analogue cathodes are designed via partial substitution of manganese (Mn) with copper (Cu) and hydrogen treatment to introduce hydroxyl (–OH) functional groups. The synergistic effect of Cu and –OH functional groups significantly enhanced the electrochemical performance of full-cell AZIBs, leading to an outstanding initial capacity of 158.5 mAh/g at 0.1 A/g, discharge plateau around 1.85 V, and capacity retention of 88.8 % after 400 cycles at 3 A/g. This enhancement is attributed to the improved material structural stability and ion transport, making the material promising for AZIB cathodes. These findings highlight the importance of synergistic material modifications for high-performance electrochemical energy storage systems.

1. Introduction

Aqueous zinc-ion batteries (AZIBs) are recognized as a viable solution for large-scale electrochemical energy storage applications [1]. Utilizing earth-abundant zinc (Zn) metal anodes and aqueous electrolytes, AZIBs offer several advantages such as low cost, safety, and eco-friendliness [1,2]. However, the development of suitable cathode materials remains a critical challenge due to the large hydrated ionic radius of Zn ions and their strong electrostatic interactions with host materials. Thus, robust structures capable of enduring the reversible insertion and extraction of Zn ions while maintaining rapid ionic transport kinetics are highly desired [1–3].

Prussian blue analogues (PBAs), $A_xM_1[M_2(CN)_6]_y{\cdot}nH_2O$, have garnered significant attention as potential cathode materials for AZIBs due to their three-dimensional open-framework structures, which facilitate the rapid insertion and extraction of Zn ions [4,5]. However, the poor capacity and electrochemical instability of PBAs in aqueous electrolytes present a significant challenge [6,7]. Prior studies have explored the incorporation of copper and nickel into the PBA framework to enhance structural stability during cycling [4,6,8]. Although these substitutions improve the cycling stability, they typically exhibit limited electrochemical activity, resulting in relatively low capacities. Additionally, while functionalization strategies have been employed to increase the specific capacity of PBAs [9], such modifications often compromise the structural integrity, leading to rapid capacity degradation and poor cycling stability.

In this study, we propose a new strategy to address the issues of low capacity and poor stability by synthesizing Mn-based PBAs (MnHCF) with copper substitution and hydrogen treatment to introduce hydroxyl (–OH) functional groups. Fig. 1 schematically depicts the synthesis process and structure of the Cu-substituted and –OH-functionalized MnHCF (donated as CH-MnHCF) cathode. The synergistic modifications can significantly improve the capacity and cycling stability of PBA cathodes in AZIBs. The CH-MnHCF cathode exhibits a high discharge plateau around 1.85 V, an initial specific capacity of 158.5 mAh/g at a current density of 0.1 A/g, and a capacity retention of 88.8 % over 400 cycles at 3 A/g. These remarkable improvements are attributed to the complementary roles of Cu substitution and –OH functionalization,

* Corresponding author.
E-mail address: Guoping.Xiong@utdallas.edu (G. Xiong).

https://doi.org/10.1016/j.matlet.2025.138013
Received 13 November 2024; Received in revised form 27 December 2024; Accepted 5 January 2025
Available online 6 January 2025

which stabilize the PBA framework, and mitigate phase transitions and material dissolution. This work underscores the potential of synergistic modification strategies to overcome the limitations of current PBA materials for efficient grid-scale energy storage.

2. Experimental

2.1. Materials synthesis

$MnSO_4$ (0.08 mol) and EDTA-K_2 (0.08 mol) are dissolved in 100 mL deionized (DI) water and the $NaFe(CN)_6$ (100 mL, 0.008 M) is added to the solution dropwise. The mixture is stirred for 30 min at room temperature and then aged for 12 h to co-precipitate. The precipitate is collected by centrifugation, washed with DI water and ethanol then dried at 80 °C for 12 h (donated as MnHCF). $CuSO_4$ (0.02 mol) is added dropwise to the redissolved MnHCF (0.5 g) solution. This solution is stirred for 30 min at room temperature and then aged for 12 h. The final precipitation is washed and dried with the same process. The dried product from the second co-precipitation process is then subjected to H_2 treatment at 300 °C for 30 min and collected as CH-MnHCF.

2.2. Materials and electrochemical characterizations

The materials and electrochemical characterization details are shown in Supplementary Material.

3. Results and discussion

The crystal structure of the CH-MnHCF is characterized by X-ray diffraction (XRD), as shown in Fig. 2a. The diffraction pattern displays well-defined peaks corresponding to the cubic phase structure of PBAs [10,11]. The left shift of characteristic peaks (as Fig. S1 shows) suggests the partial substitution of Mn by Cu, which enhances the structural stability of the material. Additionally, the pattern aligns with theoretical references for Cu-based PBAs (CuHCF) (ICDD PDF card#02-0381), indicating the incorporation of Cu atoms into the lattice.

Thermogravimetric analysis (TGA) is conducted to analyze the presence of water in the structure. The TGA curve (Fig. 2b) can be divided into three distinct stages: stage A (0–115 °C) demonstrates the release of free water; stage B (115–300 °C) marks the removal of crystal water; and stage C represents the decomposition of the PBA structure [7,12]. The CH-MnHCF exhibits significantly lower water content compared to the untreated sample, with approximately 2.6 % free water and 3.2 % crystal water, whereas the MnHCF contains 11.1 % free water and 3.5 % crystal water. This reduction in water content, particularly free water, suggests enhanced structural stability and consequently improved electrochemical properties of the treated sample [7].

Moreover, Fig. 2c presents the X-ray photoelectron spectroscopy (XPS) spectra of the CH-MnHCF. The presence of Cu, Mn, Fe, O, N, and C is confirmed, consistent with the composition of the CH-MnHCF. The Cu 2p and Mn 2p peaks indicate the successful partial Cu substitution of Mn (Fig. S2a-b). The O 1s peak confirms the introduction of –OH groups through hydrogen treatment, while the N 1s and C 1s peaks correspond to CN^- ligands, verifying the structural integrity of the PBA material [9]. The Raman spectrum (Fig. S3) of the CH-MnHCF sample shows the characteristic peaks of C≡N at 2076 and 2114 cm^{-1} [13]. The scanning electron microscopy (SEM) image in Fig. 2d shows the morphology of the CH-MnHCF material. Uniform distributed cubic-shaped nanoparticles are observed and can facilitate ion transport and fast redox reactions, enabling enhanced electrochemical performance of the material.

The galvanostatic charge–discharge profiles of CH-MnHCF- and MnHCF-based full cells are presented in Fig. 3a. The CH-MnHCF-based full cell exhibits a specific capacity of 158.5 mAh/g and a discharge plateau around 1.85 V, corresponding to reduction peak of cyclic voltammetry (CV) curves shown in Fig. 3b and Fig. S4, significantly higher than most of MnHCF-based full cells reported in prior works (Fig. S5 and Table. S1), indicating the synergetic effect of Cu substitution and –OH groups on the electrochemical performance of CH-MnHCF. The voltage profile of the CH-MnHCF-based full cell displays multi-step redox reactions, with plateaus corresponding to the redox reactions of Mn and Cu. Notably, the charge–discharge profile shows more defined voltage plateaus, suggesting improved structural stability and Zn-ion intercalation/extraction kinetics [9]. This performance improvement is attributed to the introduction of –OH groups into the cathode that reduces the Zn-ion intercalation barriers and enhances ion transport [9].

The CV analysis at different scan rates provides insights into the capacitive- and diffusion-controlled behavior of the CH-MnHCF. As shown in Fig. 3b, four prominent redox peaks (labeled Peak 1–4) are observed, each corresponding to distinct electrochemical processes. Specifically, Peak 2 and Peak 3 are associated with the Cu^{1+}/Cu^{2+} redox-active couple, while Peak 1 and Peak 4 are attributed to the Mn^{2+}/Mn^{3+} redox reaction [10,11,14]. To quantitatively assess the kinetics of these redox reactions, the relationship (Fig. 3c) between the

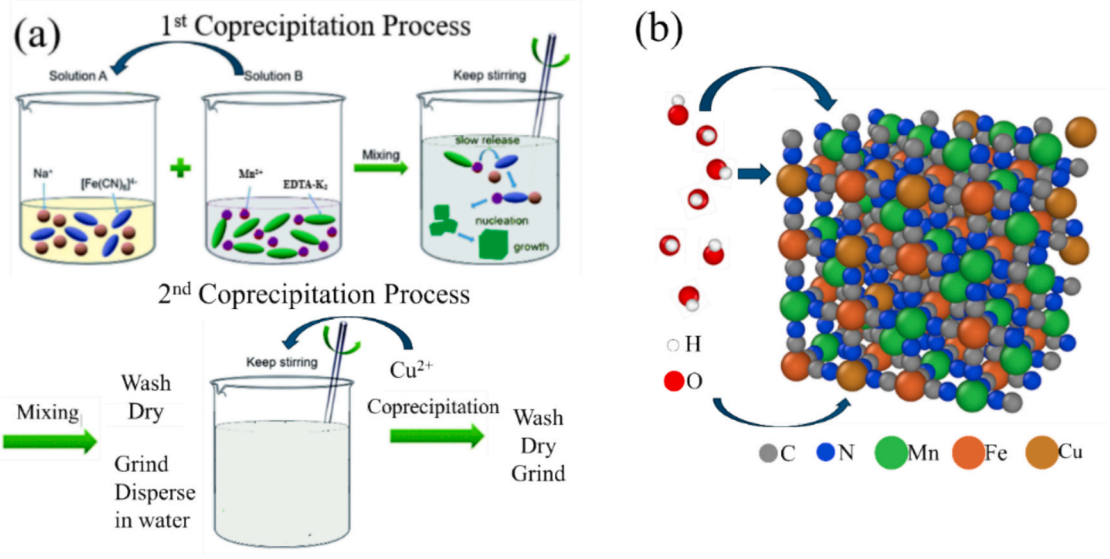

Fig. 1. (a) Schematic of the coprecipitation process of Cu-substituted Mn-based PBA cathodes. (b) Schematic of CH-MnHCF.

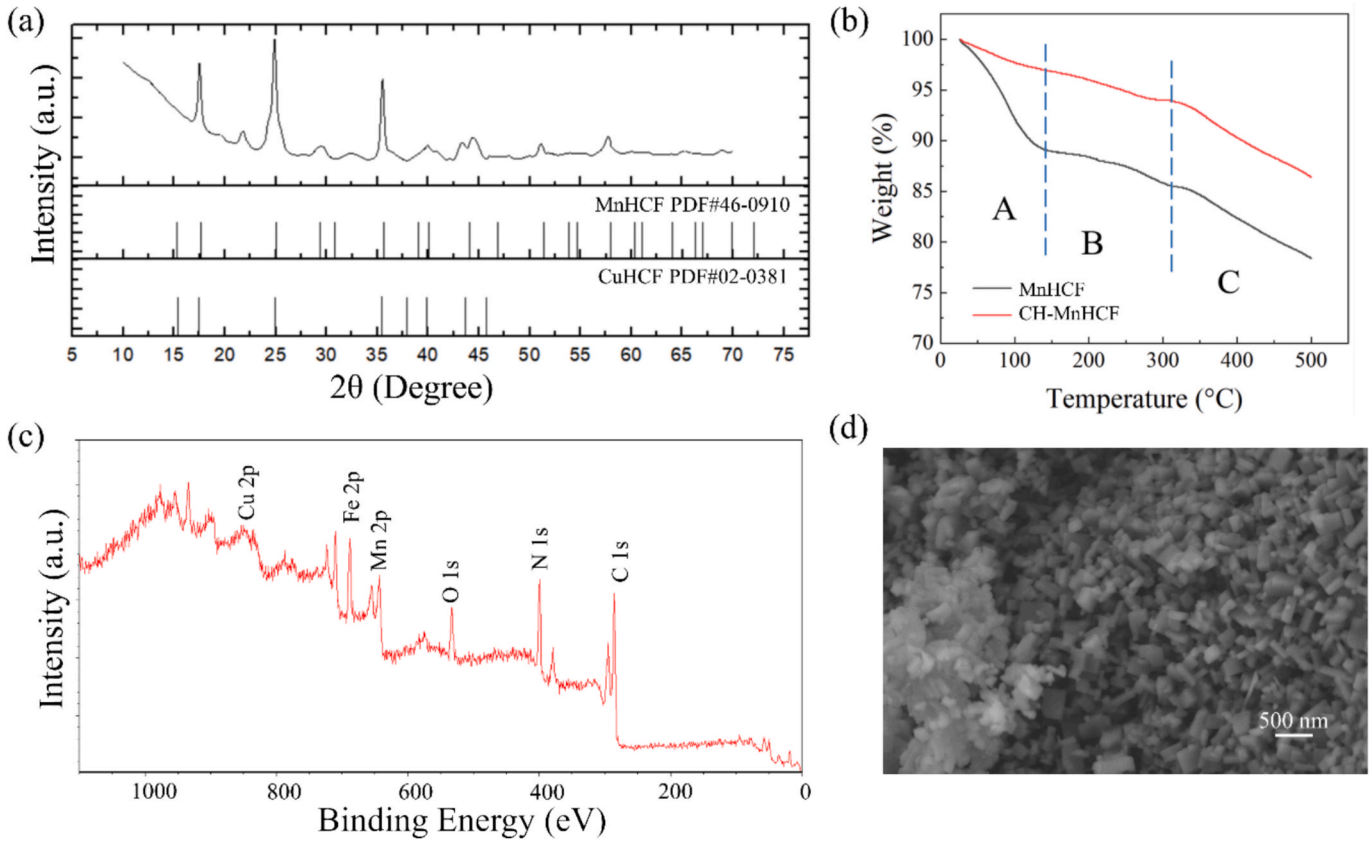

Fig. 2. (a) XRD patterns, (b) TGA curve, (c) XPS spectra, (d) SEM image of the CH-MnHCF sample.

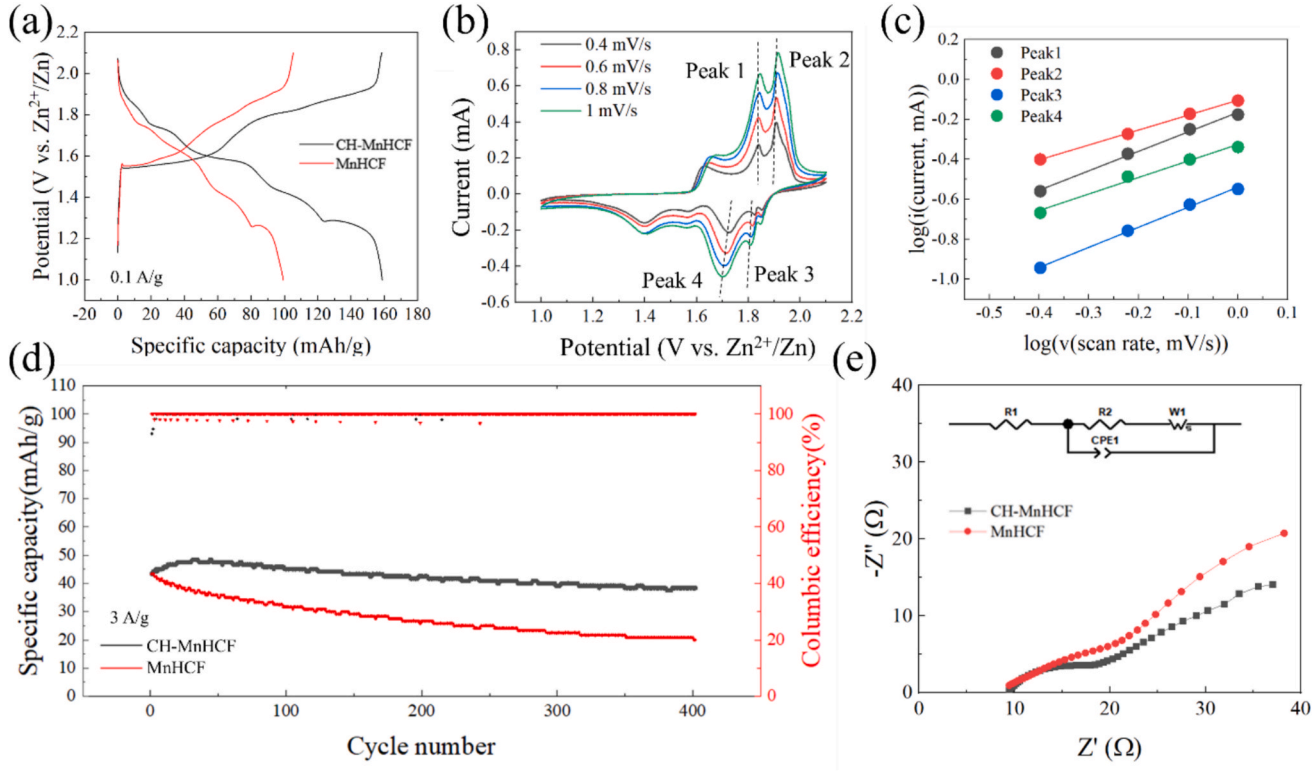

Fig. 3. (a) Galvanostatic charge–discharge profiles of full-cell AZIBs based on CH-MnHCF and MnHCF cathodes. (b) Multi-scan rates CV profiles and (c) Log(i) versus log(ν) plots of CH-MnHCF-based full cell. (d) Cyclic performance and (e) EIS profiles of CH-MnHCF- and MnHCF-based full cells.

peak current (i) and scan rate (v) is evaluated based on the power-law equation [4]: $i = av^b$, where b determines the electrochemical reaction process. The b value for each redox peak reveals important distinctions between the redox reactions of Cu and Mn. For the Cu^{1+}/Cu^{2+} redox peaks, the corresponding b values of 0.9737 (Peak 2) and 0.9861 (Peak 3) indicate a predominantly capacitive-controlled behavior, consistent with the fast kinetics of surface-limited reactions [4,6]. This suggests that –OH groups activate Cu sites in the CH-MnHCF and enhance the surface reactivity of the cathode material, allowing for rapid electron transfer during the redox process. The Mn^{2+}/Mn^{3+} redox peaks correspond to lower b values of 0.7466 (Peak 1) and 0.8273 (Peak 4), indicating a mechanism involving both diffusion- and capacitive-controlled behavior [9,10].

The CH-MnHCF-based full cell demonstrates superior cyclic stability (Fig. 3d), with a remarkable capacity retention of 88.8 %, corresponding to a discharge capacity of 38.35 mAh/g, significantly outperforming that (46.7 %) of MnHCF-based one after 400 cycles. The coulombic efficiency of the CH-MnHCF-based full cell remains close to 100 % throughout the cycling test, indicating the excellent reversibility of Zn-ion intercalation/extraction processes. The improved stability of the full cell can be attributed to enhanced structural stability due to the partial Cu substitution [10,11].

Electrochemical impedance spectroscopy (EIS) is conducted to explore the electrochemical kinetics within the CH-MnHCF-based full cell. The Nyquist plots (Fig. 3e) display distinct semicircles in the high-to-mid-frequency region, corresponding to the charge transfer resistance (R_{ct}) [4–6]. The CH-MnHCF-based full cell demonstrates a smaller semicircle than the MnHCF-based one, indicating significantly reduced R_{ct} [10]. This reduction suggests enhanced electrochemical kinetics in the CH-MnHCF cathode with improved electrical and ionic conductivity facilitated by the synergetic effect of –OH functionalization and Cu substitution.

4. Conclusion

In summary, we have successfully synthesized CH-MnHCF as a high-performance cathode material for AZIBs. The introduction of Cu stabilizes the intercalation sites and contributes to improving capacity retention during prolonged cycling. Meanwhile, the –OH functionalization reduces the intercalation barriers and facilitates Zn-ion transport. Moreover, the synergistic effect of the modifications activates Cu sites and enhances electrochemical performance. Consequently, the CH-MnHCF-based full cell exhibits a high specific capacity of 158.5 mAh g^{-1} at 0.1 A g^{-1}, a discharge plateau around 1.85 V, and excellent cycling stability with a capacity retention of 88.8 % over 400 cycles at 3 A g^{-1}. This work highlights the potential of PBA cathodes for advanced AZIB applications and provides insights into the rational design of functional materials for energy storage systems.

CRediT authorship contribution statement

Ruda Jian: Writing – original draft, Methodology, Investigation, Conceptualization. **Zhuoxun Zhang:** Writing – review & editing, Investigation, Conceptualization. **Amirarsalan Mashhadian:** Writing – review & editing, Investigation. **Roma Avhad:** Investigation. **Yun Hao:** Formal analysis. **Shuang Cui:** Supervision. **Guoping Xiong:** Writing – review & editing, Supervision, Funding acquisition, Conceptualization.

Declaration of competing interest

The authors declare that they have no known competing financial interests or personal relationships that could have appeared to influence the work reported in this paper.

Acknowledgements

G.X. acknowledges the support from University of Texas at Dallas startup fund, BEACONS Center funded by Department of Defense (DoD), and National Science Foundation (NSF) grant (No. 2324593).

Appendix A. Supplementary data

Supplementary data to this article can be found online at https://doi.org/10.1016/j.matlet.2025.138013.

Data availability

Data will be made available on request.

References

[1] P. Ruan, et al., Angew. Chem. 61 (2022).
[2] Y. Shi, et al., Small 16 (2020) 2000730.
[3] N. Wang, et al., Mater. Today Adv. 11 (2021).
[4] G. Du, et al., Energy Storage Mater. 36 (2021) 387–408.
[5] X.-Y. et al., Rare Metals (2024).
[6] Y. Li, et al., Mater. Today Energy 29 (2022).
[7] J. Liu, et al., J. Mater. Chem. A 12 (2024) 2647–2672.
[8] Y. Yang, et al., Nano Energy 99 (2022).
[9] Y. Tan, et al., Chem. Eng. J. 457 (2023).
[10] W.A. Syed, et al., J. Storage Mater. 99 (2024).
[11] Y. Zeng, et al., Angew. Chem. 61 (2022).
[12] C. Zhang, et al., Adv. Funct. Mater. 27 (2017) 1604307.
[13] A. Li, et al., ACS Appl. Energy Mater. 5 (2022) 11789–11796.
[14] M. Baghodrat, et al., Batteries 9 (2023) 170.